

Valence state of Tm in TmX ($X=S, Se, Te$) investigated by resonant inelastic x-ray scattering

I. Jarrige, H. Ishii, and Y. Q. Cai

National Synchrotron Radiation Research Center, Hsinchu 30076, Taiwan

J.-P. Rueff and C. Bonnelle

Laboratoire de Chimie Physique-Matière et Rayonnement (UMR 7614), Université Paris 6, 11 rue Pierre et Marie Curie, 75231 Paris Cedex 05, France

T. Matsumura

Department of Physics, Tohoku University, Sendai 980-8578, Japan

S. R. Shieh

Department of Earth Sciences, National Cheng Kung University, Tainan 701, Taiwan

(Received 4 February 2005; revised manuscript received 18 April 2005; published 16 August 2005)

The electronic structure of thulium monochalcogenides TmX ($X=S, Se, Te$) is investigated by x-ray absorption spectroscopy (XAS) in the partial fluorescence yield mode (PFY-XAS) and resonant x-ray emission spectroscopy around and far below the edge. These three resonant inelastic x-ray scattering (RIXS)-derived techniques yield consistent values of the thulium valency of 2.67, 2.65, and 2.70, respectively, in the mixed-valent compound TmSe. These values are in closer agreement with the valency derived from the lattice parameter measurement compared to previous x-ray photoemission spectroscopy and XAS studies. The study demonstrates that RIXS is a powerful and accurate probe of mixed-valent states in f -electron systems.

DOI: [10.1103/PhysRevB.72.075122](https://doi.org/10.1103/PhysRevB.72.075122)

PACS number(s): 78.70.En, 78.70.Ck, 71.20.Eh

I. INTRODUCTION

Rare-earth monochalcogenides have attracted a lot of interest since the 1970s, mainly because of their mixed-valence behavior, leading to remarkable optical, electrical, and magnetic properties. The valence states, and consequently the physical properties of these systems, strongly depend on their chemical composition as well as on external parameters such as temperature and pressure. Among these systems, the interplay between valence instability and electronic and magnetic degrees of freedom is at its strongest in thulium monochalcogenides TmX ($X=S, Se, Te$): in a first approximation, Tm is divalent in TmTe, trivalent in TmS, and shows fluctuating valency between 2 and 3 in TmSe. TmTe is semiconducting with an energy gap of 0.35 eV¹ and becomes metallic under pressure greater than 2 GPa.^{2,3} TmS is known to present a Kondo-like lattice behavior.^{3,4} In TmSe, both valence states of Tm²⁺ and Tm³⁺ are magnetic, and an antiferromagnetic ordering was found below 3.5 K.^{5,6}

In order to understand the unusual properties of TmX, it is therefore necessary to know precisely the Tm valency. The possibility to grow large single crystals of Tm chalcogenides with clean flat surfaces, easily obtained from cleavage,⁷ has led to numerous studies by x-ray photoemission spectroscopy (XPS).⁷⁻¹² The narrow f bands give sharp peaks in the photoemission spectra, and structures due to different valences are well separated in energy. However, the surface sensitivity introduces uncertainties in the valency extracted from the data, which is underestimated compared to the one deduced from the lattice constant. This can, in principle, be circumvented by x-ray absorption spectroscopy (XAS).^{13,14} XAS is bulk sensitive. Working at the L_3 edge provides access to the localized empty $5d$ states and thus to the rare-

earth valency. However, the XAS valency is not free from errors due to final state effects and sizable lifetime broadening in the presence of a deep core-hole. So far, a valency range of 2.55–2.79 for TmSe has been reported.⁸⁻¹⁴

In this paper, we report on the investigation of the Tm valency in TmSe using resonant inelastic x-ray scattering (RIXS)-derived techniques, namely absorption spectroscopy in the partial fluorescence yield mode (PFY-XAS) and resonant x-ray emission spectroscopies (RXES). These techniques have been applied recently to the investigation of the mixed-valence behavior in Ce- (Ref. 15) and Yb-based compounds.¹⁶⁻¹⁸ The combined bulk sensitivity and high energy resolution provide accurate spectroscopic information on the electronic structure. The present study is therefore expected to cast light on the discrepancies seen in the previous spectroscopic measurements of the valency in TmSe. We note that, in the three considered TmX compounds, the chalcogen ions accept two electrons which fill their $3p$ shell. Therefore, when Tm is supposedly trivalent while the chalcogen ion stays 2-, charge balance is recovered by considering that the third excited electron remains in the Tm $5d$ conduction states, giving rise to a $6s^0 4f^{12} 5d^1$ configuration (for intermediate valency, we assume a noninteger population of the $5d$ band). Consequently, the valency, as we refer to in this paper, also in accordance with the mainstream consensus in spectroscopy, differs from the classical notion of chemical valency. It is here rather used as a means to describe the electronic configuration of Tm.

The paper is organized as follows: The experimental details are presented in Sec. II. In Sec. III, the PFY-XAS spectra at the Tm L_3 edge are presented and discussed first, followed by the analysis of the resonant x-ray emission spectroscopy (RXES) spectra. Here the emission spectra re-

semble the density of the unoccupied $5d_{5/2}$ states, resonantly enhanced over the core hole width. These are then compared with resonant emission spectra taken with excitation energies far below the edge, where the spectra are found nearly equivalent to the absorption of the $2p_{3/2}$ states without lifetime broadening. The merits of the different approaches for extracting the Tm valency are then discussed.

II. EXPERIMENT

The measurements were performed at the Taiwan Beamline BL12XU at SPring-8 in Japan, designed primarily for inelastic x-ray scattering (IXS) studies on electronic excitations with variable energy resolution.¹⁹ A total energy resolution of 1.1 eV was chosen for the present experiment. The incident beam was monochromatized by a pair of Si(111) crystals and focused onto the sample to a spot size of $120(\text{horizontal}) \times 80(\text{vertical}) \mu\text{m}^2$ with a toroidal mirror. The emitted x rays were analyzed using a Si(531) spherically bent analyzer of 1 m radius. Energy analysis was performed in reflection geometry by moving simultaneously the analyzer and the detector in accordance with the Rowland condition. The acquisition time for one spectrum was about 10 min.

Single crystals of TmSe, TmTe, and TmS were grown by the Bridgman method in sealed tungsten crucibles using a high-frequency induction furnace. High purity Tm metal from Ames laboratory and commercial Te, Se, and S of 6N purity were used. For TmTe, the starting materials in a stoichiometric ratio were directly sealed into a crucible in vacuum by electron beam welding. For TmSe and TmS, pre-reaction was carried out in an evacuated silica tube before being sealed into a crucible to avoid evaporation of Se and S during the welding process.

III. RESULTS AND DISCUSSION

A. High-resolution absorption spectroscopy

In PFY-XAS one measures the energy dependence of the $L\alpha_1$ emission line ($3d_{5/2} \rightarrow 2p_{3/2}$) while scanning the incident energy across the Tm L_3 absorption edge. In principle, PFY-XAS allows one to obtain absorption spectra nearly free from core-hole lifetime broadening effects,^{20,21} revealing fine structures which have not previously been resolved.²² The PFY-XAS spectra measured for TmS, TmSe, and TmTe are displayed in Fig. 1 as a function of the incident energy E_1 . The conventional XAS spectrum measured for TmSe in Ref. 13 is superimposed to the PFY-XAS spectrum, illustrating the gain in resolution in our experiment. The region around the white line is proportional to the density of $5d_{5/2}$ empty states according to the dipole selection rules. The energy position of the white line, noted by a vertical solid line, is a direct signature of the thulium valency. Two shoulders can be seen in the pre-edge region of the TmS spectrum. The first structure at about 8642.5 eV can be assigned to the quadrupolar transition toward the $4f$ states. This feature is not visible in the spectra of TmSe and TmTe because of the higher intensity of the 2+ white line. The second shoulder, noted by a vertical dotted line, appears in the vicinity of the energy of

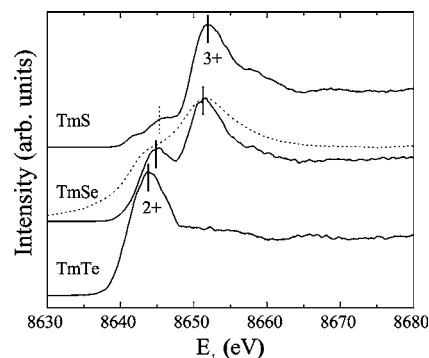


FIG. 1. PFY-XAS spectra measured for TmS, TmSe, and TmTe at the Tm L_3 edge (solid lines). The vertical solid lines indicate the energies of the Tm²⁺ and Tm³⁺ components for the different compounds. The conventional XAS spectrum obtained for TmSe in Ref. 13 (dotted line) is also shown for comparison.

the Tm²⁺ component. The presence of a residual fraction of Tm²⁺ in TmS was suggested previously by XAS and XPS studies.^{9,11} The same authors showed that TmTe inversely contains a small fraction of Tm³⁺. In the PFY-XAS spectrum of TmTe, a broad bump appears at ~ 10 eV above the 2+ white line, which can be ascribed to a weak Tm³⁺ contribution in TmTe.

In a first attempt to describe the XAS spectra in TmX compounds, we calculated the dipolar excitations at the Tm L_3 edge for both Tm²⁺ and Tm³⁺ using a multiconfiguration Dirac-Fock code (MCDF).^{23,24} The 42 lines calculated for the Tm²⁺ excitation, or the 131 lines for Tm³⁺, are summed, each line being simulated by convoluting the theoretical probability with a Lorentzian function of full width at half maximum (FWHM) equal to 1.3 eV, to account for the $3d$ core-hole lifetime in the absorption final state. These calculated excitation spectra are compared with the experimental absorption spectra obtained for TmTe and TmS in Fig. 2. All the spectra are normalized in intensity. Adjustment in energy is made by shifting the Tm²⁺ and Tm³⁺ calculated spectra by the same factor, i.e., +6 eV. The Tm³⁺ excitation transitions appear broader than the Tm²⁺ ones. This interestingly suggests that the 3+ contribution in the experimental spectra

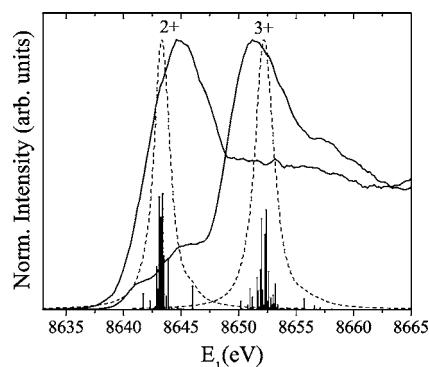


FIG. 2. PFY-XAS spectra measured for TmTe and TmS (solid lines) and calculated dipolar excitation spectra at the Tm L_3 edge (dashed lines). The spectra are normalized to the same height. Positions and heights of the lines are also given.

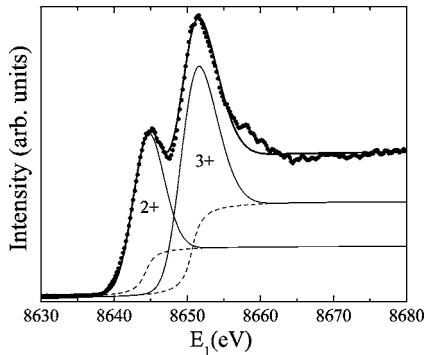


FIG. 3. The PFY-XAS spectrum obtained on TmSe (dots) is decomposed into pure 2+ and 3+ components (thin solid lines). The sum of the two components (thick solid line) and the arc-tangent continuums (dashed line) are also shown.

should be larger than the 2+ one. The broadening of the experimental spectra with respect to the calculated spectra is simultaneously due to the instrumental effects and the solid effects. The energy separation between the maxima of the experimental spectra, 8 eV, is consistent with the calculations, 8.9 eV. This good agreement indicates the rather ionic character of the bonds in these compounds and, subsequently, the validity of such an oversimplified approach. From Fig. 1, the energy splitting between the maxima of the divalent and trivalent peaks of TmSe is lower, around 6.5 eV. Furthermore, the energy position of the 2+ and 3+ components are shifted toward higher energy from TmTe to TmS, denoting a chemical shift.

The thulium valency in TmSe is determined by decomposing the PFY-XAS spectrum into pure 2+ and 3+ components. Each component is modeled by the sum of an arc-tangent function representing the continuum excitations, and a Gaussian function accounting for the strong density of 5*d* empty states present at the threshold. The inflection point of each arc-tangent line shape is constrained to coincide with the maximum of the respective Gaussian peak. The experimental spectrum is best fitted with full widths at half-maximum (FWHM) of 3.5 and 5.1 eV to the 2+ and 3+ Gaussian functions, respectively. This fit is shown in Fig. 3. A valency of 2.67 is estimated from the expression $v = 2 + [I_{3+} / (I_{2+} + I_{3+})]$, where I_{2+} and I_{3+} are the areas under the 2+ and 3+ Gaussian line shapes. We can notice that the experimental spectrum is not well accounted for by the fit in the 8656–8662 eV range. This induces an additional uncertainty on the value of the valency which we estimate to be ± 0.01 . We obtained a consistent value of 2.66 by fitting the TmSe spectrum with a weighted sum of the TmTe and TmS spectra. Nevertheless, the uncertainty on this latter value should be substantially higher than that from the former fit because of the residual 2+ and 3+ signals present in the TmS and TmTe spectra, respectively.

B. Resonant x-ray emission spectroscopy

RXES measures the radiative decay of a given atom, after primary excitation close to a resonance. It is a second-order process, well described by the Kramers-Heisenberg

equation.²² In this framework, the RXES spectra are proportional to the unoccupied local and partial density of states, resonantly enhanced over the core-hole width by the energy denominator in the Kramers-Heisenberg expression.^{25–27} We measure here the $3d_{5/2} \rightarrow 2p_{3/2}$ RXES decay process for several excitation energies across the Tm L_3 edge. In the following, the term fluorescence refers to the emission following the excitation of a core electron into the continuum, whereas the resonant signal refers to the emission from the 5*d* excitations. The RXES spectra for TmS, TmSe, and TmTe are shown in Fig. 4, as a function of the transferred energy $E_1 - E_2$, E_2 being the emitted photon energy. The emission spectra corresponding to the resonance are highlighted.

In the three TmX compounds, the variation of RXES spectra as a function of E_1 follows in intensity the PFY-XAS spectrum, shown in the inset, but the resonances corresponding to each valent state are now well separated and can be clearly identified. For comparison, the PFY-XAS spectrum is superimposed to the RXES series for TmSe (cf. dotted spectrum in Fig. 4). The trivalent signal appearing in the TmS series resonates at an incident energy corresponding to the maximum of the white line in the PFY spectrum, i.e., 8652 eV. Above the 3+ resonance energy, the emission disperses linearly, suggesting that the fluorescence regime is reached. A similar behavior is observed for the resonance of the divalent signal of the TmTe spectra. For TmSe, the spectra clearly exhibit successive resonances of the divalent and trivalent components, showing similar trend as that observed in RXES studies of ytterbium-based mixed valent compounds.^{16–18}

At their respective resonances (i.e., for $E_1 = 8644$ and 8652 eV, respectively), the TmTe and TmS spectra can be considered as pure 2+ and 3+ contributions: The parasitic 3+ and 2+ signals in TmTe and TmS are supposed to be vanishingly small at these energies. We therefore fit the TmSe spectrum at its successive 2+ and 3+ resonances (i.e., for $E_1 = 8645$ and 8651 eV) using the TmTe and TmS resonant spectra to account for the resonant 2+ and 3+ components, respectively. A replica of the resonant line shapes, scaled by an appropriated factor, is taken as the fluorescence contribution. The scaling factor is inferred from the intensity ratio between the continuum and the 5*d* transitions in the fit of the PFY-XAS spectrum at $E_1 = 8645$ and 8651 eV. The fit at $E_1 = 8645$ eV is shown in Fig. 5(a). The thulium valency in TmSe is then estimated by the same expression as in Sec. III A. I_{2+} is the intensity of the TmTe reference spectrum which fits the 2+ component in the TmSe spectrum obtained at $E_1 = 8645$ eV; I_{3+} is the intensity of the TmS reference spectrum which fits the 3+ component in the TmSe spectrum obtained at $E_1 = 8651$ eV. A valency of 2.65 is obtained.

To assess the consistency of our fitting routine, the whole series of RXES spectra acquired across the L_3 edge for TmSe was fitted using the resonant TmTe spectrum for the Tm^{2+} signal and a Gaussian profile for the fluorescence, as demonstrated in Fig. 5(b) at $E_1 = 8648$ eV. The residual spectrum is assigned to the Tm^{3+} signal. Figure 6 summarizes the results as three-dimensional maps of the isolated Tm^{2+} , Tm^{3+} , and fluorescence signals reconstructed from the series of fits. The color scales are different from one map to another in order to account for the differences in the intensity of the signals. The

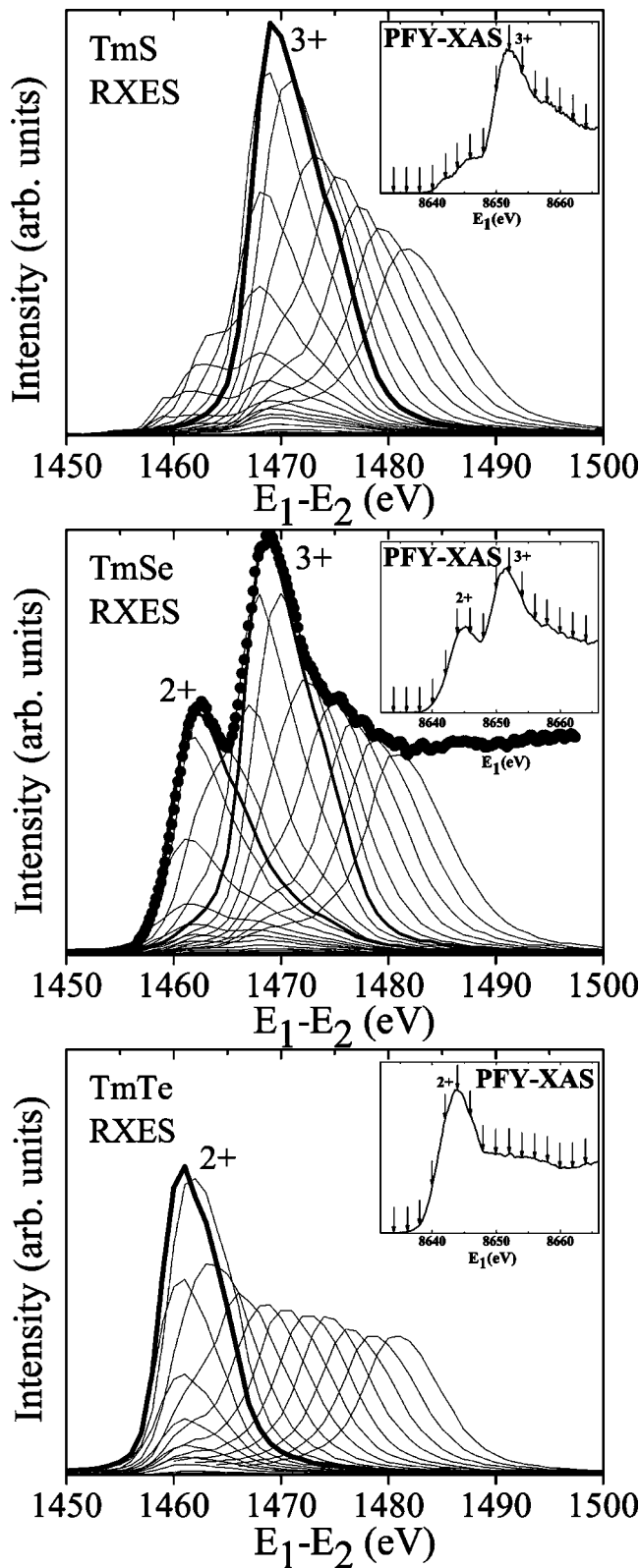


FIG. 4. Resonant emission spectra on TmS, TmSe, and TmTe obtained using incident energies indicated by the ticks in the absorption spectra as shown in the insets. The emission spectra corresponding to the 2+ and 3+ resonance are highlighted. The dotted spectrum superimposed on the RXES spectra of TmSe is the PFY-XAS spectrum.

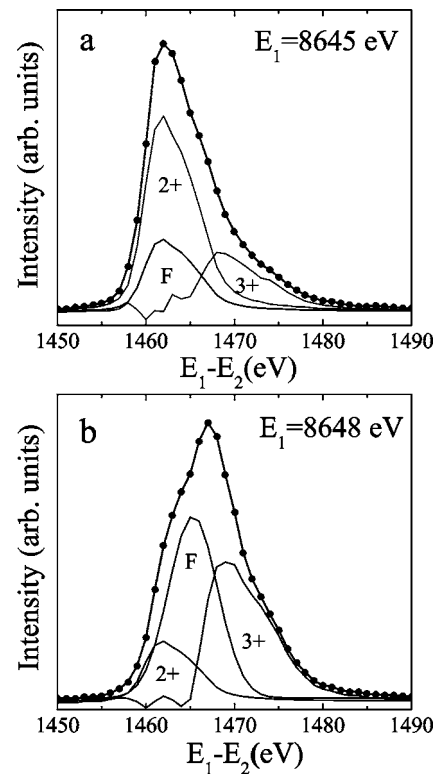


FIG. 5. Examples of the fit of RXES spectra measured for TmSe at $E_1=8645$ (a) and 8648 eV (b).

divalent and trivalent Raman features appear at constant transfer energy, while the fluorescence line linearly disperses with E_1 . The 2+ and 3+ resonances appear where the Raman dispersing features cross the fluorescence line.

As shown in Fig. 6, the validity of our fitting procedure is therefore supported by (i) a constant unfitted photon energy obtained for the fluorescence line; (ii) the transferred energies corresponding to the extracted 2+ and 3+ signals only vary within ± 1 eV; and (iii) the smooth residual 3+ signal remains always broader than the 2+ signal, which is consistent with the multiplet expectations.

C. Subthreshold resonant x-ray emission spectroscopy

We now discuss RXES spectra obtained by tuning E_1 far below the L_3 absorption edge, in the subthreshold regime. For the three TmX compounds, we observed Raman-like dispersion of the emission for incident energies down to about 62 eV below threshold. The weak emission intensity prevented further measurements at lower excitation energies. We present in Fig. 7 the emission spectra of TmSe obtained for several values of $E_1 \leq 8645$ eV, the energy of the 2+ resonance. The spectra are normalized to the same height for qualitative comparison.

The subthreshold conditions have already been shown to yield spectra which are nearly equivalent to lifetime-broadening suppressed (LBS) x-ray absorption near-edge structure (XANES).^{27,28} These conditions are achieved here when the excitation energy is ≤ 8610 eV, where the ratio between the 2+ and 3+ structures becomes constant (cf. Fig.

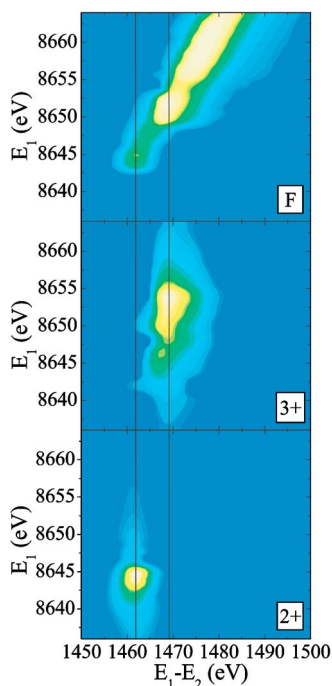


FIG. 6. (Color online) Three-dimensional mapping of the decomposed TmSe RXES spectrum in its 2+, 3+, and fluorescence components, reconstructed from the fitting procedure. The vertical lines indicate the transferred energies of the respective 2+ and 3+ Raman components.

7). It is important to note that this regime does not correspond to the nonresonant absorption at the M_5 edge, but is still related to the resonant term at the L_3 edge in the Kramers-Heisenberg formula. Moreover, the shape of the spectra mimics the L_3 PFY-XAS spectrum as can be seen from Fig. 8, where the spectrum taken at 8610 eV is compared with the PFY-XAS spectrum. This indicates that the corresponding excitations are between initial states of p character and the empty d states. The spectra also show a lower continuum tail compared to the PFY-XAS spectrum (cf. Fig. 8). This latter character constitutes a distinct advantage of using subthreshold RXES since the white lines can be characterized more accurately than in XAS, as already pointed out by Tulkki *et al.*²⁹ and Etelaniemi *et al.*³⁰

We decompose the emission spectrum obtained for TmSe at $E_1=8610$ eV into pure Tm^{2+} and Tm^{3+} components. First, the white lines region up to 1472 eV is fitted with two Gaussian peaks. This preliminary fit, though not accurate enough for the determination of the valency, aims to estimate the transitions to the continuum. Thus, the residual spectrum and its replica shifted by 6.5 eV to lower energy are respectively scaled by factors of 0.67 and 0.33, supposing initially a nominal valency of 2.67. These resulting spectra, respectively accounting for the 3+ and 2+ transitions to the continuum, are subtracted from the total emission spectrum. Finally, the residual spectrum, assigned to the sum of the 2+ and 3+ bound excitations, is then best fitted by two Gaussian line shapes of 4.7 and 6.3 eV FWHM, respectively. The fit is shown in Fig. 9. The solid lines are obtained by summing the 2+ and 3+ Gaussian curves with their respective transitions to the continuum. A valency of 2.70 is estimated from the

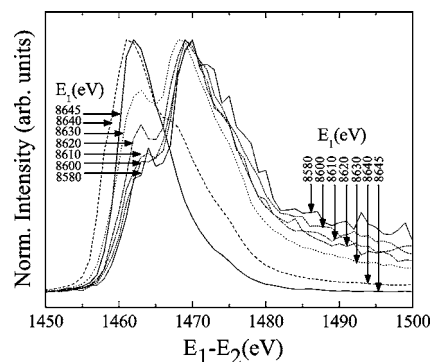


FIG. 7. Emission spectra obtained for TmSe at several values of E_1 : 8645 eV (solid line), 8640 eV (dashed line), 8630 eV (dots), 8620 eV (dash dot), 8610 eV (dash dot dot), 8600 eV (short dash), and 8580 eV (short dot).

areas under the Gaussian curves. This result was obtained with a scaling ratio between the 3+ and 2+ transitions to the continuum of 0.75/0.25. We checked that for ratios varying between 0.6/0.4 and 0.8/0.2 the valency remained constant within ± 0.01 . Using a weighted sum of the TmTe and TmS spectra to account for the TmSe subthreshold resonant emission spectrum, the same value of the valency, 2.70, is found. Nevertheless, as in the case of the weighted sum of the PFY-XAS spectrum, the uncertainty on this value is supposed higher than with the previous fit.

D. Discussion about the estimation of the thulium valency in TmSe

We now compare the thulium valencies obtained by PFY-XAS and RXES from the present studies with those derived from other experimental works. The valency of the thulium in TmSe is known to depend strongly on the stoichiometry.^{6,8,10,31} Since purely stoichiometric samples are difficult to obtain, the reported valencies sometimes arise from slightly nonstoichiometric samples. Therefore, a meaningful comparison between valencies has to consider the possible stoichiometry differences.

Besides spectroscopic data, measurements of the lattice parameter are commonly used to reliably and straightforwardly estimate the rare-earth valence state. In stoichiometric TmSe, the valency was estimated at 2.75, assuming a linear interpolation between the lattice parameters for Tm^{3+}Se and Tm^{2+}Se .^{6,8,10,31} The lattice parameter of our TmSe sample was measured by x-ray diffraction at the beamline BL10XU in SPring-8. Using a similar approach as described above, we obtain a valency of 2.75, suggesting that our sample is stoichiometric. As a matter of fact, the lattice constant was shown to systematically provide a value slightly higher than the one derived from a spectroscopic measurement.^{8-10,12-14} This discrepancy has been tentatively attributed to final-state effects in XAS and core-level XPS. In the presence of a core hole, the empty f state is pulled below the Fermi level,^{8,32} thus decreasing the effective rare-earth valence. However, such a screening effect was evidenced only for the light $4f$ rare earths, up to Nd.^{32,33} Moreover, Bianconi *et al.* suggested that the time necessary for the $4f$

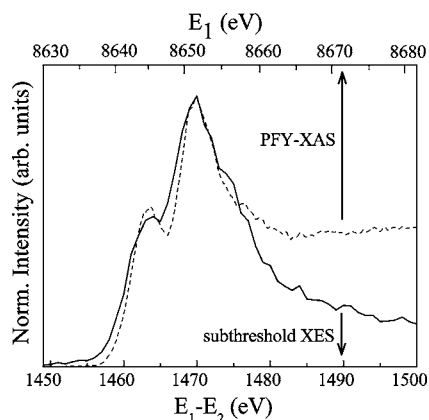


FIG. 8. Comparison of the emission spectrum obtained for TmSe at $E_1=8610$ eV (solid line), i.e., about 32.5 eV below threshold, with the PFY-XAS spectrum (dashed line).

screening process is longer than the lifetime of the excited state in XAS and core level XPS for heavy rare earths. Concerning valence band XPS, it may be tempting to ascribe the lower extracted valency to the surface sensitivity of the method, the surface layers having been shown to be mostly divalent. However, Kaindl *et al.* estimated the valency after having subtracted the surface contribution, and the resulting value was still low (2.55, cf. Table I).¹⁰

We reasonably assume here that a good agreement between the valencies obtained from a spectroscopic measurement and from the lattice constant gives consistency to the result. Therefore, the difference between these two values is proposed as indicative of the reliability of the spectroscopic study: the smaller the value of this difference, the more reliable the spectroscopic measurement. Furthermore, the value of this difference can be directly compared between different works since it is independent of the stoichiometry.

Table I presents the values of the thulium valency estimated by a spectroscopic measurement in this work and in previous works. The difference between the values inferred from the lattice parameter and from the spectroscopic analysis is indicated into brackets. The smallest difference, 0.01, arises from an XPS CFS study performed at the $N_{4,5}$ edge.^{9,11} But that difference raises up to 0.17 when the same method is applied to the M_5 edge. The lack of consistency between the two XPS CFS valencies stresses again the difficulty in obtaining reliable results with a highly surface-sensitive technique.

TABLE I. Values of the thulium valency in TmSe obtained in this work and in previous works. The numbers in brackets indicate the difference between the valency extrapolated from the lattice parameter and the one estimated by spectroscopic studies. “Sub. RXES” refers to the subthreshold RXES at $E_1=8610$ eV measurement. XPS VB stands for off-resonance valence band x-ray photoelectron spectroscopy and CFS stands for constant final state.

This work			Previous works			
PFY-XAS L_3	RXES	Sub. RXES	XAS L_3	XPS VB	XPS CFS $N_{4,5}$	XPS CFS M_5
2.67 (0.08)	2.65 (0.10)	2.70 (0.05)	2.58 (0.17) (Ref. 13)	2.56 (0.19) (Ref. 8)	2.62 (0.10) (Ref. 12)	2.63 (0.17) (Ref. 11)
			2.60 (0.15) (Ref. 14)	2.55 (0.20) (Ref. 10)	2.79 (0.01) (Refs. 9 and 11)	
				2.68 (0.12)		
				(Refs. 9 and 11)		

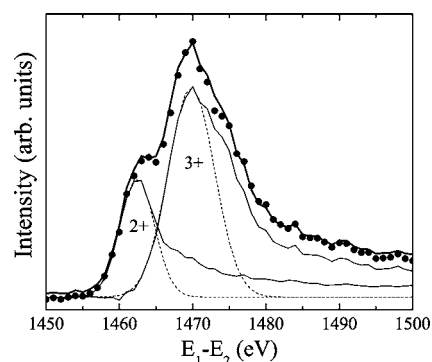


FIG. 9. The emission spectrum obtained on TmSe for $E_1=8610$ eV (dots) is decomposed into its two components (thin solid lines). The sum of both components (thick solid line) and the Gaussian line shapes (dashed line) reproducing the bound states excitations are also shown.

Our PFY-XAS, RXES, and RXES at $E_1=8610$ eV measurements give a valency smaller by respectively 0.08, 0.10, and 0.05 with the lattice constant derived value. We can consider the spread of our values as indicative of the overall error, ± 0.03 . If we set aside the difference derived from the XPS CFS $N_{4,5}$ study of Refs. 9 and 11 for the above-mentioned reason, these are the closest agreements with the lattice constant value. These results suggest that RIXS-derived techniques are among the most valuable quantitative probes of the electronic structure.

The better results obtained by the RIXS-derived techniques compared with the previous XPS studies can be explained by the difference in the probing depth of these techniques, respectively of about a few microns and a few nanometers. The energy resolution gain of the PFY-XAS experiment in comparison with the previous XAS studies is shown to enhance significantly the reliability of the measurement. The slightly better measurement provided by the subthreshold resonant emission compared to PFY-XAS may, on the one hand, illustrate the accuracy gain arising from the lower relative intensity of the transitions to the continuum states. Consequently, the maxima corresponding to the transitions to the $5d$ states are more precisely determined than by PFY-XAS. On the other hand, this value should be more sensitive to the fit procedure than in the case of RXES, where no continuum subtraction is required. In RXES, one can selectively enhance and disentangle some intermediate states from the overall unoccupied density of states, it is

therefore possible to measure and resolve the signals arising from both valencies with a high accuracy.

IV. CONCLUSION

The three RIXS-derived techniques provide consistent values of the valency of the thulium in the mixed-valent compound TmSe. The excellent agreement with the lattice constant measurement ensures both the accuracy and reliability of the measurement. Our study further demonstrates that subthreshold RXES can be used to derive quantitative infor-

mation on the electronic structure as accurately as RXES around the edge does.

ACKNOWLEDGMENTS

The authors thank Dr. N. Sata for help during the x-ray diffraction measurement at BL10XU, SPring-8. This work was carried out at SPring-8 under the experiment number C04B12XU-1500N and was partly supported by NSRRC, the National Science Council of Taiwan under Grant No. NSC 92-2112-M-213-012.

-
- ¹R. Suryanarayanan, G. Guntherodt, J. L. Freeouf, and F. Holtzberg, *Phys. Rev. B* **12**, 4215 (1975).
- ²J. Tang, T. Kosaka, T. Matsumura, T. Matsumoto, N. Mori, and T. Suzuki, *Solid State Commun.* **100**, 571 (1996).
- ³T. Matsumura, T. Kosaka, J. Tang, T. Matsumoto, H. Takahashi, N. Mori, and T. Suzuki, *Phys. Rev. Lett.* **78**, 1138 (1997), and references therein.
- ⁴E. Bucher, K. Andres, F. J. di Salvo, J. P. Maita, A. C. Gossard, A. S. Cooper, and G. W. Hull, Jr., *Phys. Rev. B* **11**, 500 (1975).
- ⁵B. Batlogg, *Phys. Rev. B* **23**, 1827 (1981).
- ⁶F. Holtzberg, T. Penney, and R. Tourmier, *J. Phys. (Paris), Colloq.* **40**, C5-314 (1979).
- ⁷M. Campagna, E. Bucher, G. K. Wertheim, D. N. E. Buchanan, and L. D. Longinotti, *Phys. Rev. Lett.* **32**, 885 (1974).
- ⁸G. K. Wertheim, W. Eib, E. Kaldis, and M. Campagna, *Phys. Rev. B* **22**, 6240 (1980).
- ⁹Y. Ufuktepe, S. Kimura, T. Kinoshita, K. G. Nath, H. Kumigashira, T. Takahashi, T. Matsumura, T. Suzuki, H. Ogasawara, and A. Kotani, *J. Phys. Soc. Jpn.* **67**, 2018 (1998).
- ¹⁰G. Kaindl, C. Laubschat, B. Reihl, R. A. Pollak, N. Martensson, F. Holtzberg, and D. E. Eastman, *Phys. Rev. B* **26**, 1713 (1982).
- ¹¹S. Kimura, Y. Ufuktepe, K. G. Nath, T. Kinoshita, H. Kumigashira, T. Takahashi, T. Matsumura, T. Suzuki, H. Ogasawara, and A. Kotani, *J. Magn. Magn. Mater.* **177-181**, 349 (1998).
- ¹²S.-J. Oh, J. W. Allen, and I. Lindau, *Phys. Rev. B* **30**, 1937 (1984).
- ¹³H. Launois, M. Rawiso, E. Holland-Moritz, R. Pott, and D. Wohlleben, *Phys. Rev. Lett.* **44**, 1271 (1980).
- ¹⁴A. Bianconi, S. Modesti, M. Campagna, K. Fischer, and S. Stizza, *J. Phys. C* **14**, 4737 (1981).
- ¹⁵J.-P. Rueff, C. F. Hague, J.-M. Mariot, L. Journel, R. Delaunay, J.-P. Kappler, G. Schmerber, A. Derory, N. Jaouen, and G. Krill, *Phys. Rev. Lett.* **93**, 067402 (2004).
- ¹⁶C. Dallera, M. Grioni, A. Shukla, G. Vanko, J. L. Sarrao, J. P. Rueff, and D. L. Cox, *Phys. Rev. Lett.* **88**, 196403-1 (2002).
- ¹⁷C. Dallera, E. Annese, J.-P. Rueff, A. Palenzona, G. Vanko, L. Braicovich, A. Shukla, and M. Grioni, *Phys. Rev. B* **68**, 245114 (2003).
- ¹⁸E. Annese, J.-P. Rueff, G. Vanko, M. Grioni, L. Braicovich, L. Degiorgi, R. Gusmeroli, and C. Dallera, *Phys. Rev. B* **70**, 075117 (2004).
- ¹⁹Y. Q. Cai, P. Chow, C. C. Chen, H. Ishii, K. L. Tsang, C. C. Kao, K. S. Liang, and C. T. Chen, *AIP Conf. Proc.* **705**, 340 (2004).
- ²⁰K. Hämäläinen, D. P. Siddons, J. B. Hastings, and L. E. Berman, *Phys. Rev. Lett.* **67**, 2850 (1991).
- ²¹P. Carra, M. Fabrizio, and B. T. Thole, *Phys. Rev. Lett.* **74**, 3700 (1995).
- ²²J.-P. Rueff, L. Journel, P.-E. Petit, and F. Farges, *Phys. Rev. B* **69**, 235107 (2004).
- ²³J. Bruneau, *J. Phys. B* **16**, 4135 (1983).
- ²⁴C. Bonnelle, G. Giorgi, and J. Bruneau, *Phys. Rev. B* **50**, 16255 (1994).
- ²⁵J. A. Carlisle, Eric L. Shirley, E. A. Hudson, L. J. Terminello, T. A. Callcott, J. J. Jia, D. L. Ederer, R. C. C. Perera, and F. J. Himpsel, *Phys. Rev. Lett.* **74**, 1234 (1995).
- ²⁶M. Magnuson, J.-E. Rubensson, A. Fohlisch, N. Wassdahl, A. Nilsson, and N. Martensson, *Phys. Rev. B* **68**, 045119 (2003).
- ²⁷H. Hayashi, Y. Udagawa, W. A. Caliebe, and C.-C. Kao, *Chem. Phys. Lett.* **371**, 125 (2003).
- ²⁸Y. Udagawa, H. Hayashi, K. Tohji, and T. Mizushima, *J. Phys. Soc. Jpn.* **63**, 1713 (1994).
- ²⁹J. Tulkki and T. Åberg, *J. Phys. B* **15**, L435 (1982).
- ³⁰V. Etelaniemi, K. Hämäläinen, S. Manninen, and P. Suortti, *J. Phys.: Condens. Matter* **4**, 879 (1992).
- ³¹B. Batlogg, H. R. Ott, E. Kaldis, W. Thoni, and P. Wachter, *Phys. Rev. B* **19**, 247 (1979).
- ³²G. Creelius, G. K. Wertheim, and D. N. E. Buchanan, *Phys. Rev. B* **18**, 6519 (1978).
- ³³J. C. Fuggle, M. Campagna, Z. Zolnierrek, R. Lasser, and A. Platau, *Phys. Rev. Lett.* **45**, 1597 (1980).